Supplementary Information for "Ultrafast charge localization in a stripe-phase nickelate"

G. Coslovich,[1] B. Huber,[1] W.-S. Lee,[2] Y.-D. Chuang,[3] Y. Zhu,[1] T. Sasagawa,[4] Z. Hussain,[3] H. A. Bechtel,[3] M. C. Martin,[3] Z.-X. Shen,[2] R. W. Schoenlein[1] & R. A. Kaindl[1]

[1]*Materials Sciences Division, E. O. Lawrence Berkeley National Laboratory, 1 Cyclotron Road, Berkeley, CA 94720, U.S.A.,*

[2]*SIMES, SLAC National Accelerator Laboratory, and Stanford University, Menlo Park, CA 94025, U.S.A.,*

[3]*Advanced Light Source, E. O. Lawrence Berkeley National Laboratory, 1 Cyclotron Road, Berkeley, CA 94720, U.S.A.,*

[4]*Materials and Structures Laboratory, Tokyo Institute of Technology, Kanagawa 226-8503, Japan*

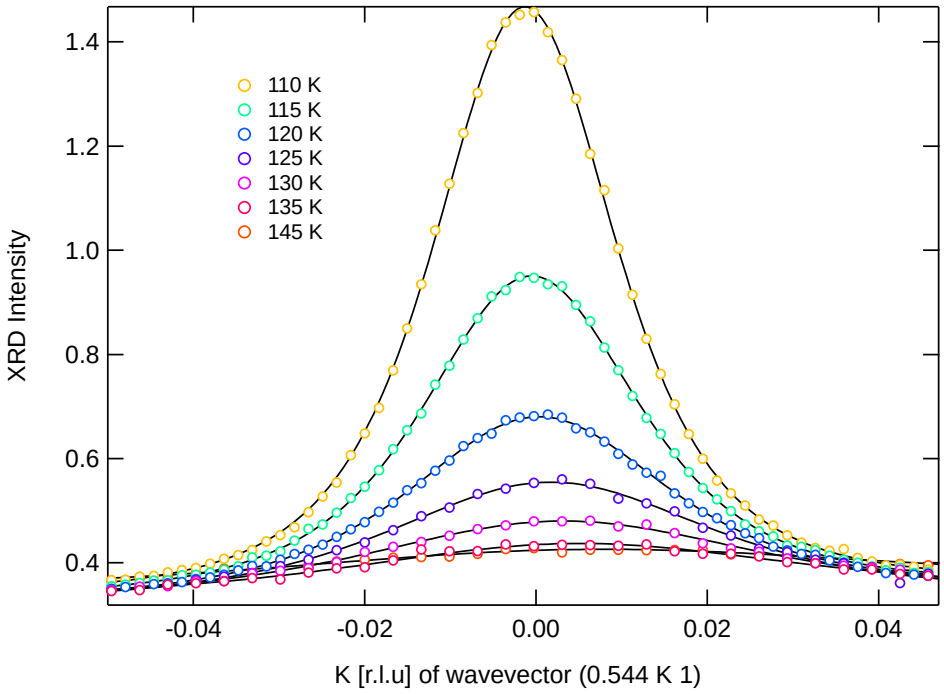

Supplementary Figure S1 | Temperature Dependence of Charge-Order XRD Signal. Profiles of the X-ray diffraction peak centered at (0.544 0 1) along the wavevector coordinate K (circles), indicated in reciprocal lattice units (r.l.u.), for different temperatures. Solid lines: fits to a squared-Lorentzian function. The temperature range is chosen to highlight the accuracy of the fitting procedure above T_{CO}, where the peak intensity drops and the system exhibits critical stripe fluctuations.

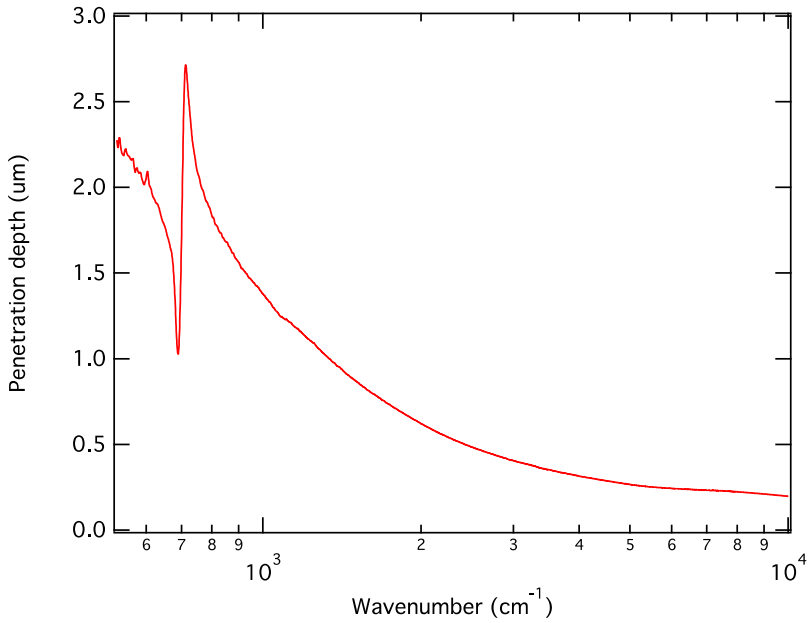

Supplementary Figure S2 | Spectral Dependence of the Penetration Depth. The penetration depth is calculated from the extinction coefficient of our LSNO sample at 30 K. The frequency axis is shown in logarithmic scale. Optical properties are calculated through the Kramers-Kronig constrained variational method from the measured optical reflectivity, as explained in the Methods section.

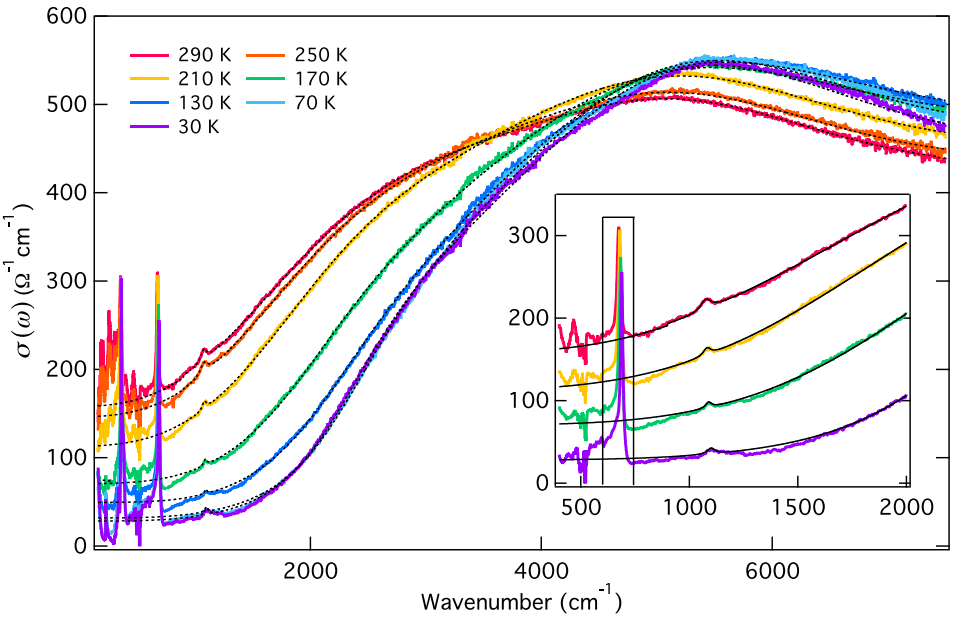

Supplementary Figure S3 | Multi-oscillator Model of the Electronic Background. Optical conductivity at different temperatures and corresponding fits obtained from the multi-oscillator model (see text). The inset shows a zoom in the area of the Ni-O stretching phonon mode.

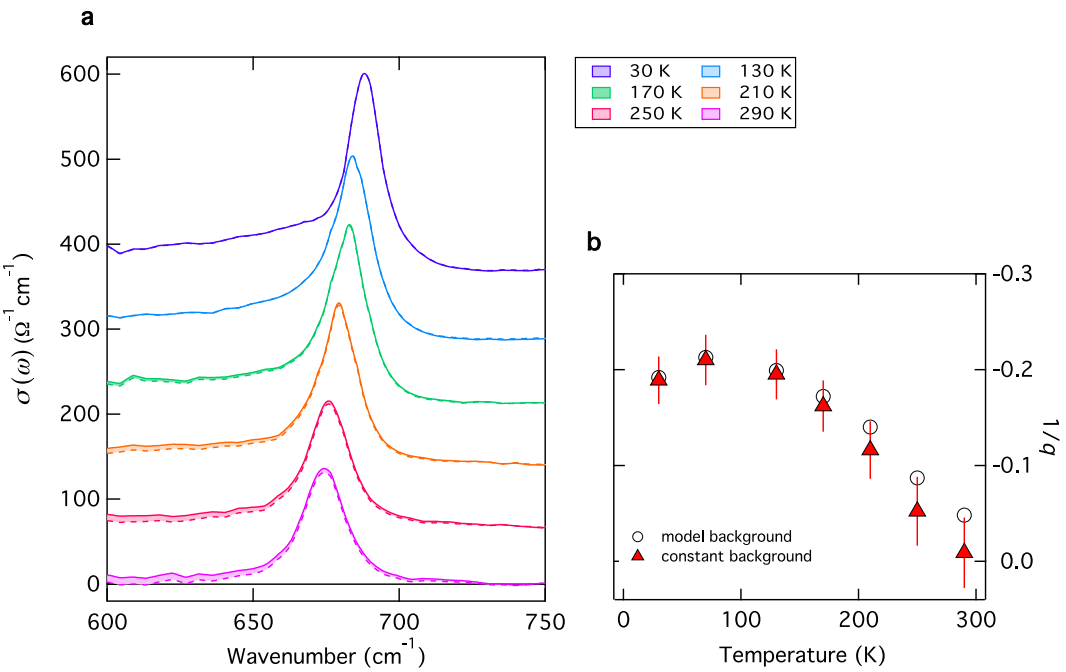

Supplementary Figure S4 | Effect of Background Subtraction on the Ni-O Phonon Profiles. a, Optical conductivity (solid lines) of the Ni-O stretching phonon mode after subtraction of the multi-oscillator model background, along with the curves (dashed lines) shown in Fig. 2a of the main text. The shaded areas highlight the deviations due to the different background subtraction procedure. The curves are offset vertically for clarity and better comparison. **b,** Comparison of the asymmetry parameter q^{-1} obtained from this procedure to the one used in the main text (Fig. 2c). The error bars represent the 95% confidence interval in extracting the fitting parameters and they account for the deviations between the two methods.

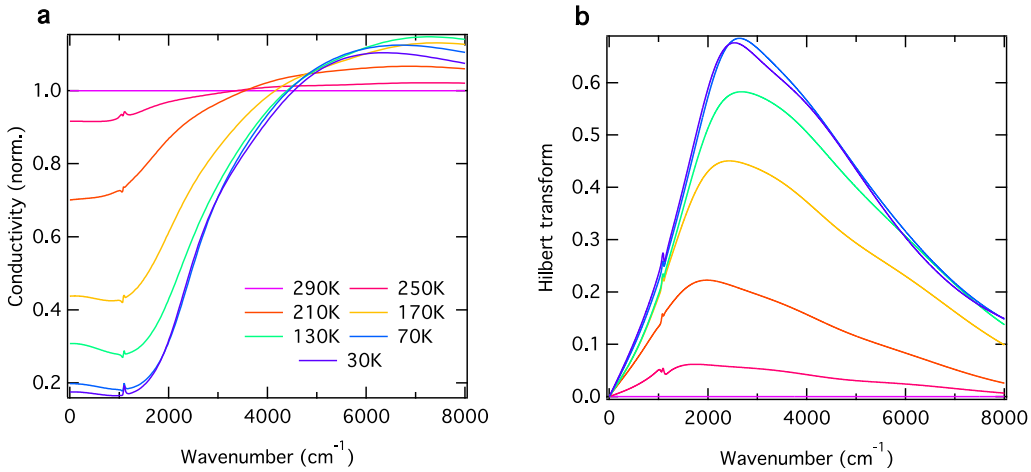

Supplementary Figure S5 | Normalized Conductivity and Hilbert Transform. a, Conductivity curves of the model background normalized to the room temperature conductivity. **b,** Hilbert transform of the normalized conductivity.

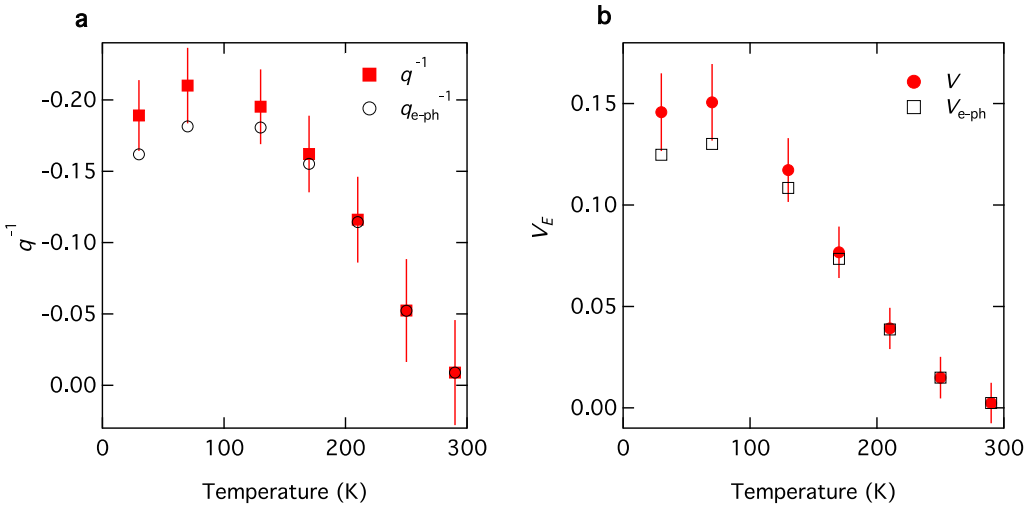

Supplementary Figure S6 | Fano Model Calculations for Non-Constant Background. a, Asymmetry parameter q^{-1} (open symbol) obtained after the inclusion of self-energy effects due to the non-constant electronic background. The results from the simplified Fano formalism (featureless background) are shown for comparison (solid symbol). **b,** Calculated strength of the electron-phonon coupling V_E obtained from the Fano formalism for both constant (solid symbol) and non-constant (open symbol) electronic background cases. Error bars represent the 95% confidence interval in extracting the fitting parameters.

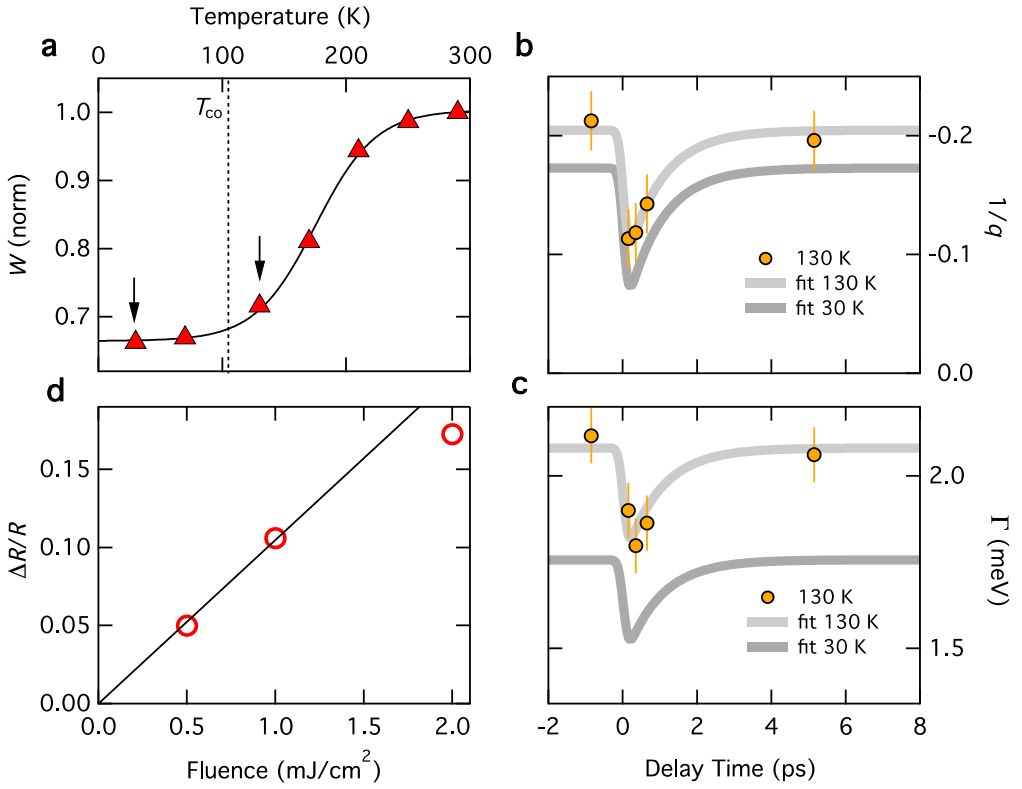

Supplementary Figure S7 | Temperature and Fluence Dependence of Time-Resolved Data. a, Spectral weight temperature dependence (same data as in Fig. 1c). The arrows highlight the 30 K data discussed in the main text along with the 130 K data discussed here. **b** and **c,** Fitting parameters obtained from the 130 K photo-induced data on the Ni-O stretching phonon mode. **d,** Fluence dependence of the $\Delta R/R$ signal peak measured at λ = 5 um. Error bars represent the 95% confidence interval in extracting the fitting parameters.

Supplementary Methods

Details on the Application of the Fano Theory

Background Subtraction. The Fano model describes the effect of a coherent interaction between a narrow resonance and a broad continuum. An important aspect of the data analysis based on the Fano model is the careful subtraction of the broad continuum background. In this work we subtracted a constant background, measured at 800 cm^{-1}, i.e., ≈ 8 linewidths away from the Ni-O stretch phonon mode (Figs. 2 and 4). This procedure is justified by the fact that the broad continuum is a slowly varying function in the range of interest (600-750 cm^{-1}). In the following we show that similar results are obtained when performing a more sophisticated background subtraction. Uncertainties arising from the use of a constant background subtraction procedure are included in the error bars used in Figs. 2 and 4 of the main text.

A set of Lorentz oscillators can reproduce the room temperature optical conductivity at frequencies higher than 900 cm^{-1}, namely

$$\sigma(\omega) = \epsilon_0 \sum_{i=1}^{N} \frac{\omega_{Pi}^2 \omega}{i(\omega_i^2 - \omega^2) + \omega/\tau_i}, \quad \text{(S1)}$$

where the i-th oscillator is characterized by a plasma frequency ω_{Pi}, a scattering rate $1/\tau_i$ and a resonance frequency ω_i. ϵ_0 is the permittivity of free space and the formulas are expressed in SI units. To fit the data at lower temperatures, where the pseudogap opens in the optical conductivity we adopt the phenomenological formula used in Refs. 39,40 where the above conductivity σ is multiplied by the gap function

$$\mathcal{F}(\omega) = \xi_0 + (1 - \xi_0)\frac{1}{2}\left(1 + \tanh\left(\frac{\omega - 2\Delta}{2\zeta}\right)\right), \quad \text{(S2)}$$

where ξ_0 indicates the filling factor, Δ the pseudogap frequency and ζ the gap width. By using only two main oscillators in the 1000-8000 cm^{-1} spectral range and a damped Drude oscillator, this model provides a good fit to the experimental data over a very large spectral energy range (see Supplementary Figure S3). Supplementary Figure S4a shows the profiles of the Ni-O stretching mode where the above multi-oscillator electronic background has been subtracted. This procedure gives very similar results as obtained after subtracting a constant background (see dashed lines in Supplementary Figure S4a), becoming essentially indistinguishable below 170 K. The only notable

difference is a small offset in the values of the Fano asymmetry parameter q^{-1} at high temperatures. The results of both subtraction procedures are compared in Supplementary Figure S4b. We observe that the overall experimental features in the temperature dependence remain the same. Similar results with even smaller deviations are obtained for the time-dependent case. This convinced us to adopt the simpler constant background subtraction in the main text and include the small deviations due to the simplified procedure in the error bars of Figs. 2 and 4 of the main text.

Fano analysis in the presence of a frequency-dependent electronic background. In the Fano model the Hamiltonian matrix of the interacting system can be written as[26]

$$\begin{aligned} &< \phi|\mathcal{H}|\phi > = E_0 \\ &< \psi_E|\mathcal{H}|\phi > = V_E \\ &< \psi_{E'}|\mathcal{H}|\psi_E > = E\ \delta(E - E') \end{aligned} \tag{S3}$$

where $\mathcal{H}$ is the Hamiltonian, $|\phi >$ represents the phonon mode of energy E_0, and the term V_E represents the coherent interaction between the mode and the continuum of states $|\psi_E >$ at energy E. The intensity profile measured in the conductivity spectra follows the Fano shape[26]

$$\sigma(\varepsilon) = \frac{\epsilon_0 A}{\Gamma(q^2-1)}\left[\frac{(q+\varepsilon)^2}{1+\varepsilon^2} - 1\right], \tag{S4}$$

where A indicates the net integrated spectral weight of the optical transition, $\varepsilon = (\hbar\omega - E_0 - \delta E)/\Gamma$ is the reduced energy, $\Gamma = \pi|V_E|^2 + \gamma$ is the Fano linewidth, and γ indicates the intrinsic linewidth due to screening and anharmonic effects. In the above, the line shift δE is given by

$$\delta E = \frac{1}{\pi}\wp \int dE' \frac{\pi|V_{E'}|^2}{E-E'} \tag{S5}$$

and the Fano asymmetry parameter is written as

$$q = \frac{<\phi|T|i> + \wp \int dE' \frac{V_{E'} < \psi_{E'}|T|i>}{E-E'}}{\pi V_E < \psi_E|T|i>}, \tag{S6}$$

where $|i >$ represents the set of initial states for the optical transition. Both the line shift δE and the second term in the asymmetry parameter q are generally referred to as self-energy effects[26] and are proportional to the Hilbert transform, $H(E) = \frac{1}{\pi}\wp \int dE' \frac{D(E')}{E-E'}$,

of the joint density of states $D(E)$, as pointed out by Cerdeira et al.[41] The asymmetry parameter in Eq. (S6) can thus be rewritten as a sum $q = q_{\text{e-ph}} + q_{\text{H}}$, where only the first term is inversely proportional to the coupling. In the main text we assumed a featureless electronic background, for which the Hilbert transform is zero and the relation $q^{-1} = {q_{\text{e-ph}}}^{-1} \propto V_E$ holds, i.e., the asymmetry parameter can be used as a direct measurement of the electron-phonon coupling strength. This is still a reasonable assumption when the background electronic conductivity is a slowly varying function of the photon energy, as in our case. In the following we explicitly calculate the q_{H} term and show that possible deviations due to this approximation are within the experimental error bars and cannot be the cause for the measured temperature dependence of q.

In evaluating the q_{H} term we proceed by normalizing $D(E)$ to the room temperature density of states, $D_{\text{n}}(E)$. If we assume $D_{\text{n}}(E)$ to be constant in energy, we can rewrite

$$q_{\text{H}} = \frac{H(E)}{D(E)} = \frac{\wp \int dE' \frac{D(E')/D_{\text{n}}(E')}{E-E'}}{\pi D(E)/D_{\text{n}}(E)} \,. \tag{S7}$$

The assumption of a constant density of states at room temperature may neglect a constant offset in ${q_{\text{H}}}^{-1}$ (small since q is very close to zero at 290 K). However the temperature dependent features are taken into account exactly, e.g. the opening of a pseudogap in the density of states, which can ultimately cause a temperature dependence of q_{H}.

The Kubo-Greenwood formula[42], $\sigma(\hbar\omega) = \frac{\pi e^2}{m^2 \omega} \left|\mathbf{p^2}\right| D(\hbar\omega)$, where $\mathbf{p}$ is the momentum operator, can be used to relate the normalized density of states to the normalized conductivity, obtaining a readily usable formula:

$$q_{\text{H}} = \frac{\wp \int dE' \frac{\sigma(E')/\sigma_{\text{n}}(E')}{E-E'}}{\pi \sigma(E)/\sigma_{\text{n}}(E)} \,. \tag{S8}$$

Here the use of the Kubo-Greenwood formula (valid at low temperatures) is justified by the large energy scale of the spectral features involved (with the pseudogap being of the order $2\Delta \approx 0.5$ eV), which makes thermal population effects negligible.

The normalized conductivities, $\sigma(E)/\sigma_{\text{n}}(E)$, for each temperature are shown in Supplementary Figure S5a, while the corresponding Hilbert transform is shown in Supplementary Figure S5b. Around 700 cm^{-1} the Hilbert transform remains below 0.15

for each temperature, yielding a $q_{\mathrm{H}} < 1$. This leads to small deviations due to the inclusion of the ${q_{\mathrm{H}}}^{-1}$ term when comparing q to $q_{\text{e-ph}}$ (see Supplementary Figure S6a). Importantly, we note that the deviations remain within the error bars of q^{-1}. This result supports the proportionality $q^{-1} \cong {q_{\text{e-ph}}}^{-1} \propto V_E$ used in the main text.

To quantitatively determine the Fano interaction V_E we can take into account the temperature-dependent optical transition amplitudes in Eq. (S6). The transition amplitudes can be evaluated by using the measured optical conductivity and thus we obtain the relation

$$V_E = \frac{q^{-1}}{\pi}\sqrt{\frac{\sigma_{\mathrm{ph}}}{\sigma_{\mathrm{el}}}}\,, \tag{S9}$$

where the phonon conductivity σ_{ph} is determined from the net spectral weight of the phonon transition A of the Fano profile, and σ_{el} is the electronic background. Supplementary Figure S6b shows the results of this calculation underscoring the dramatic increase of the interaction at lower temperatures. Also in this case we note that the deviations remain small when the effect of a non-constant background is included in the calculations.

Temperature and pump fluence dependence. In the following we include some experimental details about the temperature and fluence dependence of the pump-probe data presented in this work.

To verify that the photo-induced suppression of the Fano effect is genuinely connected to the pseudogap physics (with onset temperature T^* ≈ 200 K) and is not related to the long-range stripe formation at T_{CO} (≈ 105 K), we verified that the photo-induced effects are substantially the same at 130 K as at 30 K. These two temperatures are chosen because the transferred spectral weight is almost the same (Supplementary Figure S7a), but the long-range order is suppressed at 130 K. The results obtained from the Fano fits of the time-resolved data at 130 K are summarized and compared to the data at 30 K in Supplementary Figures. S7b-c. The photo-induced changes of both the asymmetry parameter and the linewidth are compatible with those measured at 30 K, underscoring the irrelevance of the long-range order in the modulation of the electron-phonon coupling. An offset in the equilibrium linewidth is observed at 130 K, mostly due to enhanced incoherent interactions (e.g. anharmonicity). At room temperature, where the

pseudogap is almost completely closed, we did not obtain a measurable time-resolved signal within the noise level for the phonon mode, suggesting a much weaker perturbation of the Ni-O stretching mode.

The pump fluence dependence of the pseudogap suppression was also analysed (Supplementary Figure S7d). All the measurements presented in the main text have been performed at 1 mJ/cm^2 since it is the highest fluence that does not cause non-linear (saturation) effects. Measurements at 0.5 mJ/cm^2 did not show substantial differences except for a lower signal-to-noise ratio.

Supplementary References

39. Homes, C. C., Timusk, T., Bonn, D. A., Liang, R. & Hardy, W. N. Optical properties along the c-axis of $YBa_2Cu_3O_{6+x}$, for x = 0.50 → 0.95 evolution of the pseudogap. *Physica C: Superconductivity* **254**, 265–280 (1995).

40. Kuzmenko, A. Guide to RefFit. *http://optics.unige.ch/alexey/reffit_files/Manual.pdf* (2012)

41. Cerdeira, F., Fjeldly, T. A. & Cardona, M. Effect of Free Carriers on Zone-Center Vibrational Modes in Heavily Doped p-type Si. II. Optical Modes. *Physical Review B* **8**, 4734–4745 (1973).

42. Dressel M. & Gruner G. *Electrodynamics of Solids.* Cambridge University Press (2002).